# Introduction to the Analysis and Design of Offshore Structures– An Overview

N. Haritos
*The University of Melbourne, Australia*

ABSTRACT: This paper provides a broad overview of some of the key factors in the analysis and design of offshore structures to be considered by an engineer uninitiated in the field of offshore engineering. Topics covered range from water wave theories, structure-fluid interaction in waves to the prediction of extreme values of response from spectral modeling approaches. The interested reader can then explore these topics in greater detail through a number of key references listed in the text.

## 1 INTRODUCTION

The analysis, design and construction of offshore structures is arguably one of the most demanding sets of tasks faced by the engineering profession. Over and above the usual conditions and situations met by land-based structures, offshore structures have the added complication of being placed in an ocean environment where hydrodynamic interaction effects and dynamic response become major considerations in their design. In addition, the range of possible design solutions, such as: ship-like Floating Production Systems, (FPSs), and Tension Leg Platform (TLP) deep water designs; the more traditional jacket and jack-up (space truss like) oil rigs; and the large member sized gravity-style offshore platforms themselves (see Fig. 1), pose their own peculiar demands in terms of hydrodynamic loading effects, foundation support conditions and character of the dynamic response of not only the structure itself but also of the riser systems for oil extraction adopted by them. Invariably, non-linearities in the description of the hydrodynamic loading characteristics of the structure-fluid interaction and in the associated structural response can assume importance and need be addressed. Access to specialist modelling software is often required to be able to do so.

This paper provides a broad overview of some of the key factors in the analysis and design of offshore structures to be considered by an engineer uninitiated in the field of offshore engineering. Reference is made to a number of publications in which further detail and extension of treatment can be explored by the interested reader, as needed.

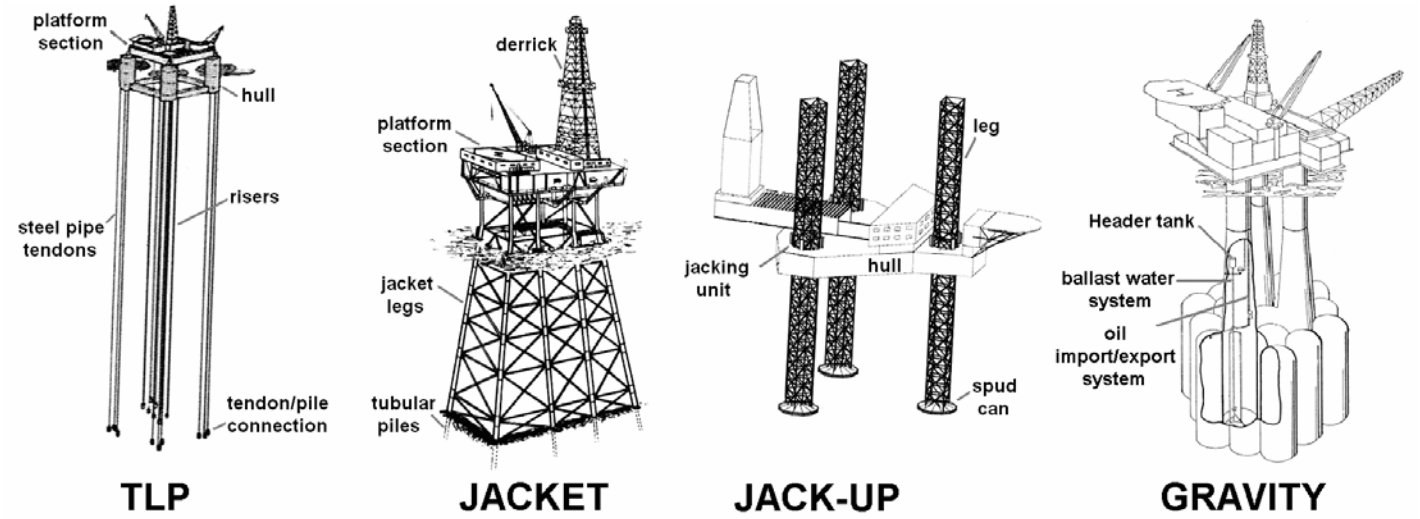


Figure1: Sample offshore structure designs

## 2 OFFSHORE ENGINEERING BASICS

A basic understanding of a number of key subject areas is essential to an engineer likely to be involved in the design of offshore structures, (Sarpkaya & Isaacson, 1981; Chakrabarti, 1987; Graff, 1981; DNS-OS-101, 2004).

These subject areas, though not mutually exclusive, would include:

- Hydrodynamics
- Structural dynamics
- Advanced structural analysis techniques
- Statistics of extremes

amongst others.

In the following sections, we provide an overview of some of the key elements of these topic areas, by way of an introduction to the general field of offshore engineering and the design of offshore structures.

### 2.1 *Hydrodynamics*

Hydrodynamics is concerned with the study of water in motion. In the context of an offshore environment, the water of concern is the salty ocean. Its motion, (the kinematics of the water particles) stems from a number of sources including slowly varying currents from the effect of the tides and from local thermal influences and oscillatory motion from wave activity that is normally wind-generated.

The characteristics of currents and waves, themselves would be very much site dependent, with extreme values of principal interest to the LFRD approach used for offshore structure design, associated with the statistics of the climatic condition of the site of interest, (Nigam & Narayanan: Chap. 9, 1994).

The topology of the ocean bottom also has an influence on the water particle kinematics as the water depth changes from deeper to shallower conditions, (Dean & Dalrymple, 1991). This influence is referred to as the "shoaling effect", which assumes significant importance to the field of coastal engineering. For so-called deep water conditions (where the depth of water exceeds half the wavelength of the longest waves of interest), the influence of the ocean bottom topology on the water particle kinematics is considered negligible, removing an otherwise potential complication to the description of the hydrodynamics of offshore structures in such deep water environments.

A number of regular wave theories have been developed to describe the water particle kinematics associated with ocean waves of varying degrees of complexity and levels of acceptance by the offshore engineering community, (Chakrabarti, 2005). These would include linear or Airy wave theory, Stokes second and other higher order theories, Stream-Function and Cnoidal wave theories, amongst others, (Dean & Dalrymple, 1991).

The rather confused irregular sea state associated with storm conditions in an ocean environment is often modelled as a superposition of a number of Airy wavelets of varying amplitude, wavelength, phase and direction, consistent with the conditions at the site of interest, (Nigam & Narayanan, Chap. 9, 1994). Consequently, it becomes instructive to develop an understanding of the key features of Airy wave theory not only in its context as the simplest of all regular wave theories but also in terms of its role in modelling the character of irregular ocean sea states.

#### 2.1.1 *Airy Wave Theory*

The surface elevation of an Airy wave of amplitude *a*, at any instance of time *t* and horizontal position *x* in the direction of travel of the wave, is denoted by $\eta(x,t)$ and is given by:

$$\eta(x,t) = a\cos(\kappa x - \omega t) \tag{1}$$

where wave number $\kappa = 2\pi / L$ in which $L$ represents the wavelength (see Fig. 2) and circular frequency $\omega = 2\pi / T$ in which $T$ represents the period of the wave. The celerity, or speed, of the wave $C$ is given by $L/T$ or $\omega/\kappa$, and the crest to trough wave-height, $H$, is given by $2a$.

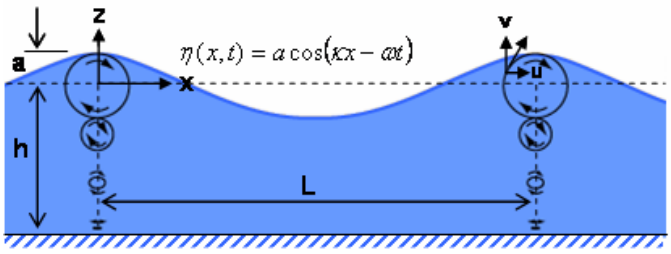

Figure 2: Definition diagram for an Airy wave

The alongwave $u(x,t)$ and vertical $v(x,t)$ water particle velocities in an Airy wave at position $z$ measured from the Mean Water level (MWL) in depth of water $h$ are given by:

$$u(x,t) = \frac{a\omega\cosh(\kappa(z+h))}{\sinh(\kappa h)}\cos(\kappa x - \omega t) \tag{2}$$

$$v(x,t) = \frac{a\omega\sinh(\kappa(z+h))}{\sinh(\kappa h)}\sin(\kappa x - \omega t) \tag{3}$$

The dispersion relationship relates wave number $\kappa$ to circular frequency $\omega$ (as these are not independent), via:

$$\omega^2 = g\kappa\tanh(\kappa h) \tag{4}$$

where $g$ is the acceleration due to gravity (9.8 m/s$^2$).

The alongwave acceleration $\dot{u}(x,t)$ is given by the time derivative of Equation (2) as:

$$\dot{u}(x,t) = \frac{a\omega^2 \cosh(\kappa(z+h))}{\sinh(\kappa h)} \sin(\kappa x - \omega t) \quad (5)$$

It should be noted here that wave amplitude, $a$, is considered small (in fact negligible) in comparison to water depth $h$ in the derivation of Airy wave theory.

For deep water conditions, $\kappa h > \pi$, Equations (2) to (5) can be approximated to:

$$u(x,t) = a\omega e^{\kappa z} \cos(\kappa x - \omega t) \quad (6)$$

$$v(x,t) = a\omega e^{\kappa z} \sin(\kappa x - \omega t) \quad (7)$$

$$\omega^2 = g\kappa \quad (8)$$

$$\dot{u}(x,t) = a\omega^2 e^{\kappa z} \sin(\kappa x - \omega t) \quad (9)$$

This would imply that the elliptical orbits of the water particles associated with the general Airy wave description in Equations (2) and (3), would reduce to circular orbits in deep water conditions as implied by Equations (6) and (7).

## 2.2 *Higher order and stretch wave theories*

A number of "finite amplitude" wave theories have been proposed that seek to improve on the restriction of the 'negligible wave amplitude compared with water depth' assumption in the definition of Airy waves. The most notable of these include second and higher order (eg fifth order) Stokes waves, (Chakrabarti, 2005), waves based upon Fenton's stream function theory (Rienecker & Fenton, 1981), and Cnoidal wave theory (Dean & Dalrymple, 1991).

The introduction of the so-called "stretch" theory by Wheeler (1970), as implied in its name, uses the results of Airy wave theory under the negligible amplitude assumption as a basis, to map these results into the finite region of their extent from the sea bottom to their current position of wave elevation. (This is essentially achieved by replacing "$z$" with "$z/(1+\eta/h)$" in the Airy wave equations presented above).

Chakrabarti (2005) refers to alternative concepts and some second order modifications for achieving "stretching" corrections to basic Airy wave theory results, though not commonly adopted, can nonetheless be used for this purpose. with Le Mahaute's original description and that of a numbers of other authors in this field)

Le Mahaute (1969) provided a chart detailing applicability of various wave theories using wave steepness versus depth parameter in his description, reproduced here in Figure 3. (The symbol for depth of water is taken as $d$ instead of $h$ to be consistent.)

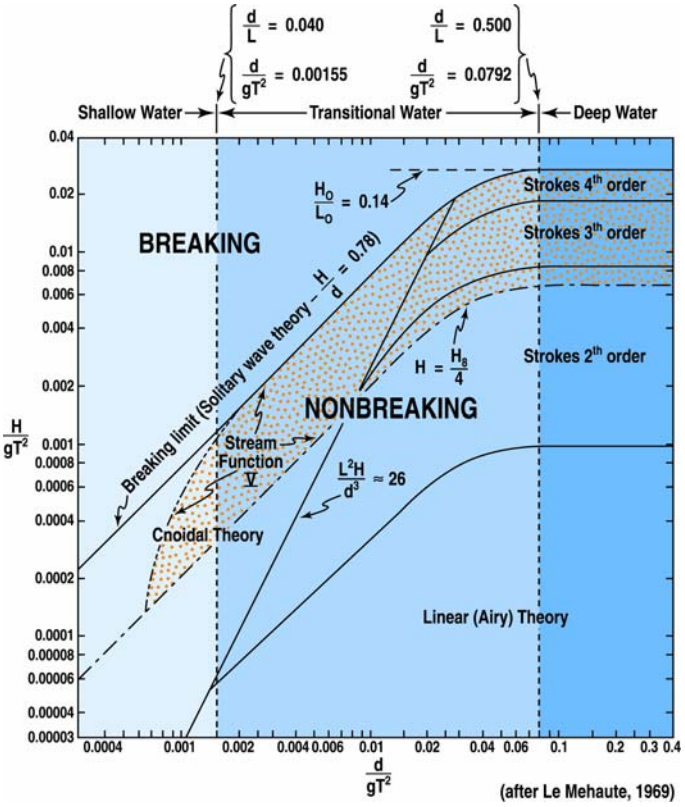


Figure 3: Applicability of Wave Theories

## 2.3 *Irregular Sea States*

Ocean waves are predominantly generated by wind and although they appear to be irregular in character, tend to exhibit frequency-dependent characteristics that conform to an identifiable spectral description.

Pierson and Moskowitz (1964), proposed a spectral description for a fully-developed sea state from data captured in the North Atlantic ocean, viz:

$$S(\omega) = \frac{\alpha g^2}{\omega^5} e^{-\beta\left(\frac{\omega_o}{\omega}\right)^4} \quad (10)$$

where $\omega = 2\pi f$, $f$ is the wave frequency in Hertz, $\alpha = 8.1 \times 10^{-3}$, $\beta = 0.74$, $\omega_o = g/U_{19.5}$ and $U_{19.5}$ is the wind speed at a height of 19.5 m above the sea surface, (corresponding to the height of the anemometers on the weather ships used by Pierson and Moskowitz).

Alternatively, equation (10) can be expressed as:

$$S_\eta(f) = \frac{0.0005}{f^5} e^{\frac{-5}{4}\left(\frac{f_p}{f}\right)^4} \quad (11)$$

in which $f_p = 1.37/U_{19.5}$, is the frequency in Hertz at peak wave energy in the spectrum and where $H_s = 4\sigma_\eta = 0.021U_{19.5}^2$. (Note that the variance of a random process can be directly obtained from the area under its spectral density variation, hence the basis for the relationship for $\sigma_\eta \approx 0.005U_{19.5}^2$, from the P-M spectral description quoted above). Figure 4 depicts sample plots of the Pierson-Moskowitz (P-M) spectrum for a selection of wind speed values, $U_{19.5}$.

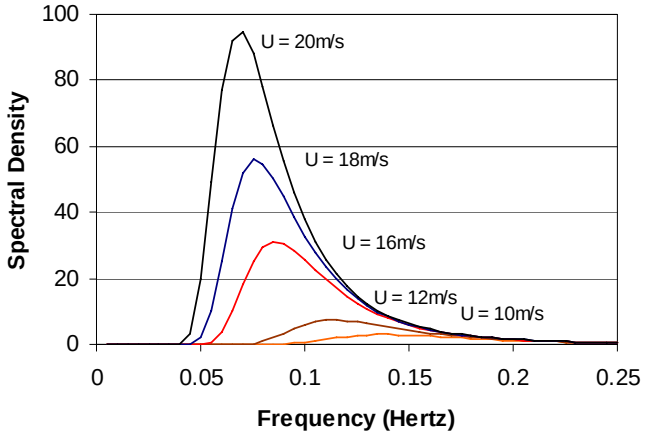


Figure 4: Sample Pierson-Moskowitz Wave Spectra

An irregular sea state can be considered to be composed of a Fourier Series of Airy wavelets conforming to a nominated spectral description, such as the P-M spectral variation.

Then wave height $\eta(t)$ can be expressed as

$$\eta(t) = \sum_{n=0}^{N/2} \left( \sqrt{\frac{2.S_\eta(f)}{T}} \sin\left( \frac{2\pi nt}{T} - \phi_n \right) \right) \qquad (12)$$

where η(t) is represented by a series of points ($\eta_1$, $\eta_2$, $\eta_3$, …, $\eta_M$) at a regular time step of dt for M points where T = M.dt here represents the time length of record, and $\phi_n$ is a random phase angle between 0 and 2π. (Equation (12) offers a convenient approach towards numerically simulating sea states conforming to a desired spectral variation via the Fast Fourier Transform. Such sea state descriptions can then be adopted in numerical studies that take into account non-linear characteristics and features that would otherwise not be considered for convenience).

## 3 ENVIRONMENTAL LOADS ON OFFSHORE STRUCTURES

### 3.1 *Wind Loads*

Wind loads on offshore structures can be evaluated using modelling approaches adopted for land-based structures but for conditions pertaining to ocean environments. The distinction here is that an open sea presents a lower category of roughness to the free-stream wind, which leads to a more slowly varying mean wind profile with height and to lower levels of turbulence intensity than encountered on land. As a consequence, wind speed values at the same height above still water level (for offshore conditions) as those above ground level (for land-based structures) for nominal storm conditions, tend to be stronger and lead to higher wind loads. (Figure 5 provides a diagrammatic representation of this mean wind speed variation).

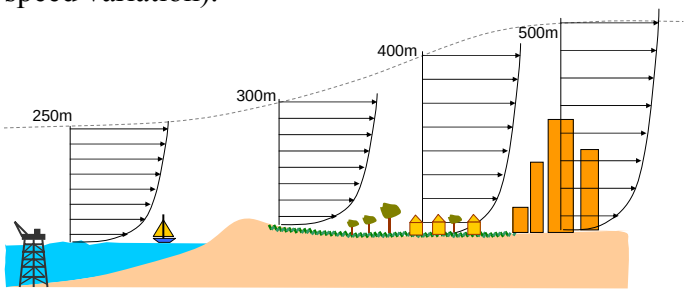


Figure 5: Variation of mean wind speed with height

For free-stream wind speed, $U_G$, at gradient height, $z_G$ (the height outside the influence of roughness on the free-stream velocity), the mean wind speed at level z above the surface, $\overline{U}(z)$, is given by the power law profile

$$\overline{U}(z) = U_G\left(\frac{z}{z_G}\right)^\alpha = \overline{U}_{ref}\left(\frac{z}{z_{ref}}\right)^\alpha \le U_G \qquad (13)$$

where $\alpha$ is the power law exponent and "ref" refers to a reference point typically chosen to correspond to 10m.

Table I compares values for key descriptive parameters, $\alpha$ and $z_G$, for different terrain conditions, including those for rough seas.

Table I Wind speed profile parameters

| Terrain | Rough Sea | Grassland | Suburb | City centre |
|---|---|---|---|---|
| $\alpha$ | 0.12 | 0.16 | 0.28 | 0.40 |
| $z_G$ (m) | 250 | 300 | 400 | 500 |

The drag force, $F_W(t)$, exerted on a bluff body (eg such as the exposed frontal deck area of an offshore oil rig), by turbulent wind pressure effects can be evaluated from

$$F_W(t) = \frac{1}{2}\rho_a C_D A V^2(t) \qquad (14)$$

where $\rho_a$ is the density of air (1.2 kg/m$^3$), $A$ is the exposed area of the bluff body, $C_D$ is the drag coefficient associated with the bluff body shape/geometry, and $V(t)$ is wind speed at the location of the bluff body.

### 3.2 *Wave Loads*

The wave loads experienced by offshore structural elements depend upon their geometry, (the size

of these elements relative to the wavelength and their orientation to the wave propagation), the hydrodynamic conditions and whether the structural system is compliant or rigid. Structural elements that are large enough to deflect the impinging wave (diameter to wavelength ratio, $D/L > 0.2$) undergo loading in the diffraction regime, whereas smaller, more slender, structural elements are subject to loading in the Morison regime.

### 3.2.1 *Morison's Equation*

The alongwave or in-line force per unit length acting on the submerged section of a rigid vertical surface-piercing cylinder, $f(z,t)$, from the interaction of the wave kinematics at position z from the MWL, (see Fig. 6), is given by Morison's equation, viz:

$$f(z,t) = f_I(z,t) + f_D(z,t) \tag{15}$$

where $f_I(z,t) = (\pi/4)\rho C_M D^2 \dot{u}(z,t)$ and $f_D(z,t) = 0.5\rho C_D D u(z,t)|u(z,t)|$ represent the inertia and drag force contributions in which $C_M$ and $C_D$ represent the inertia and drag force coefficients, respectively, $\rho$ is the density of sea water and $D$ is the cylinder diameter.

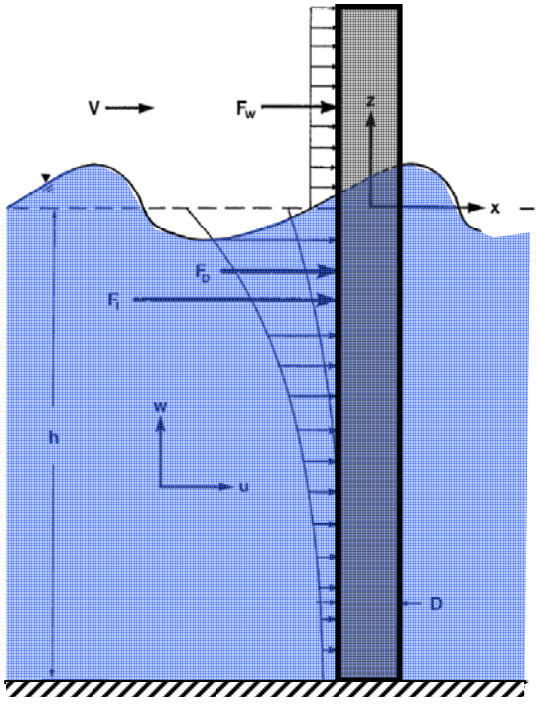


Figure 6: Wave Loading on a Surface-Piercing Bottom-Mounted Cylinder

Force coefficients $C_M$ and $C_D$ are found to be dependent upon Reynold's number, *Re*, Keulegan-Carpenter number, *KC*, and the $\beta$ parameter, viz:

$$KC = \frac{u_m T}{D};\ \beta = \frac{Re}{KC} \tag{16}$$

where $u_m$ = the maximum alongwave water particle velocity. It is found that for $KC < 10$, inertia forces progressively dominate; for $10 < KC < 20$ both inertia and drag force components are significant and for $KC > 20$, drag force progressively dominates.

Sarpkaya's (1976) original tests conducted on instrumented horizontal test cylinders in a U-tube with a controlled oscillating water column remain to be the most comprehensive exploration of Morison force coefficients in the published literature.

Figures 7 and 8, derived from these results provide an indication of the variation of these force coefficients with respect to *KC* and *Re*. As a rule of thumb, it can be stated that $C_M$ decreases as $C_D$ increases, and vice versa, and that both values generally lie in the range 0.8 to 2.0. The drag force coefficient is also influenced by roughness on the cylinder. (Marine growth is particularly troublesome in this regard as it not only increases the effective diameter of a cylinder, but the increase in roughness generally leads to an increase in drag coefficient, $C_D$).

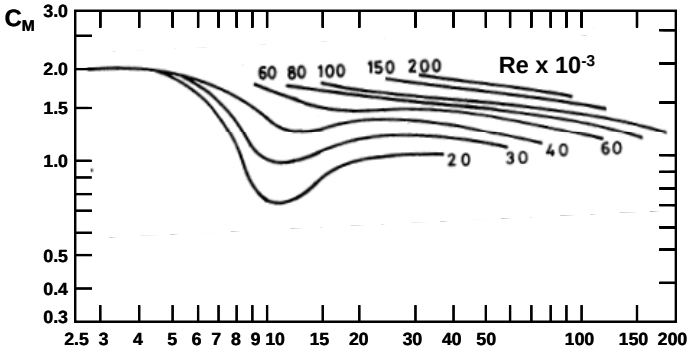


Figure 7: Inertia force coefficient dependence on flow parameters

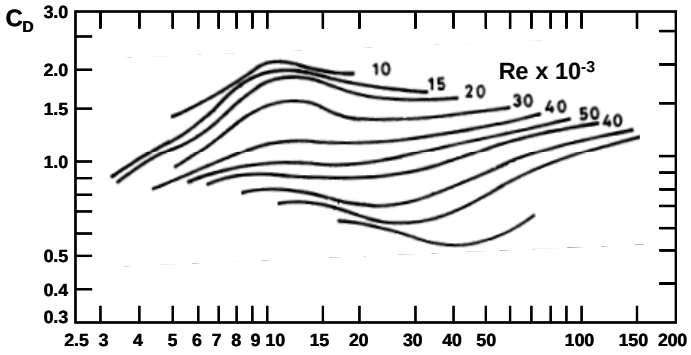


Figure 8: Drag force coefficient dependence on flow parameters

The Morison equation has formed the basis for design of a large proportion of the world's offshore platforms - a significant infrastructure asset base, so its importance to offshore engineering cannot be understated. Appendix I provides a derivation of the

Morison wave loads for a surface-piercing cylinder for small amplitude Airy waves and illustrates key features of the properties of the inertia and drag force components.

### 3.3 *Transverse (Lift) wave loads*

Transverse or lift wave forces can occur on offshore structures as a result of alternating vortex formation in the flow field of the wave. This is usually associated with drag significant to drag dominant conditions ($KC > 15$) and at a frequency associated with the vortex street which is a multiple of the wave frequency for these conditions. The vortex shedding frequency, $n$, is determined by the Strouhal number, $N_S$, whose value is dependent upon the structural member shape and $Re$, (typically ~0.2 for a circular cylinder in the range $2.5 \times 10^2 < \mathrm{Re} < 2.5 \times 10^5$), and which is defined by

$$N_S = \frac{nD}{U_m} \tag{17}$$

where $U_m$ is the maximum alongwave water particle velocity and D is the transverse dimension of the member under consideration (eg diameter of the cylinder).

The lift force per unit length, $f_L$, can be defined via

$$f_L = \frac{1}{2}\rho C_L D U_m \left|U_m\right| \tag{18}$$

where $C_L$ is the Lift force coefficient that is dependent upon the flow conditions. Again, Sarpkaya's (1976) original tests conducted on instrumented horizontal test cylinders in a U-tube with a controlled oscillating water column, also provide a comprehensive exploration of the lift force coefficient, from which the results depicted in Figure 9 have been obtained. (It should be noted here, that in the case of flexible structural members, when the vortex shedding frequency $n$ coincides with the member natural frequency of oscillation, the resultant vortex-induced vibrations give rise to the so-called "lock-in" mechanism which is identified as a form of resonance).

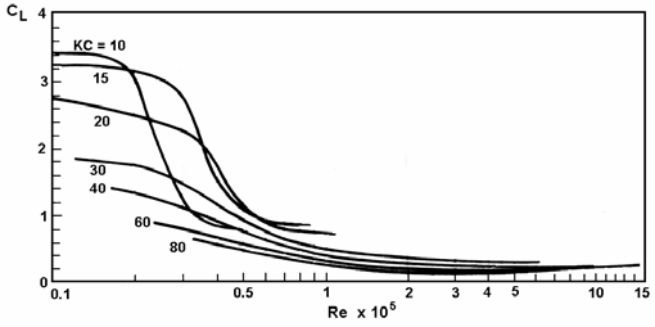


Figure 9: Lift force coefficient dependence on flow parameters

### 3.4 *Diffraction wave forces*

Diffraction wave forces on a vertical surface-piercing cylinder (such as in Fig. 6) occur when the diameter to wavelength ratio of the incident wave, $D/L$, exceeds 0.2 and can be evaluated by integrating the pressure distribution derived from the time derivative of the incident and diffracted wave potentials, (MacCamy & Fuchs, 1954). Integrating the first moment of the pressure distribution allows evaluation of the overturning moment effect about the base. Results obtained for the diffraction force $F(t)$ and overturning moment $M(t)$ are given by:

$$F(t) = \frac{2\rho g H}{\kappa^2} A(\kappa a)\tanh(\kappa h)\cos(\omega t - \alpha) \tag{19}$$

$$M(t) = \frac{2\rho g H}{\kappa^2} A(\kappa a) \left[\kappa h \tanh(\kappa h) + \sec h(\kappa h) - 1\right]\cos(\omega t - \alpha) \tag{20}$$

where

$$A(\kappa a) = \left[J_1'^{\,2}(\kappa a) + Y_1'^{\,2}(\kappa a)\right]^{-\frac{1}{2}};\ \alpha = \tan^{-1}\left(\frac{J_1'(\kappa a)}{Y_1'(\kappa a)}\right) \tag{21}$$

in which $a$ is the radius of the cylinder ($D/2$), ($'$) denotes differentiation with respect to radius $r$, $J_1$ and $Y_1$ represent Bessel functions of the first and second kinds of $1^{st}$ order, respectively. It should be noted that specialist software based upon panel methods, is normally necessary to investigate diffraction forces on structures of arbitrary shape, (eg WAMIT, SESAM).

### 3.5 *Effect of compliancy (relative motion)*

In the situation where a structure is compliant (ie not rigid) and its displacement in the alongwave direction at position $z$ from the free surface at time $t$ is given by $x(z,t)$, then the form of Morison's equation modified under the "relative velocity" formulation, becomes:

$$f(z,t) = \frac{\pi}{4}\rho.C_M.D^2\dot{u}(z,t) - \frac{\pi}{4}\rho.(C_M - 1).D^2\ddot{x}(z,t) + \frac{1}{2}\rho.C_D.D.(u(z,t) - \dot{x}(z,t))\left|u(z,t) - \dot{x}(z,t)\right| \tag{22}$$

Consider the structure concerned to be of the form of the surface-piercing cylinder depicted in Figure 6. Consider the displacement at the MWL to be $x_o(t)$ and the primary mode shape of response of the cylinder to be $\psi(z)$, with $\psi(0) = 1$, then the cylinder motion can be considered to satisfy that obtained from the equation of a single-degree-of-freedom (SDOF) oscillator, given by:

$$m\ddot{x}_o(t) + c\dot{x}_o(t) + kx_o(t) \approx \int_{-h}^{0} \Psi(z)\, f(z,t)\, dz \qquad (23)$$

where the integration has been taken to the MWL in lieu of $\eta(t)$, and at x = 0, as an approximation. Coefficients *m, c,* and *k* represent the equivalent mass, viscous damping and restraint stiffness of the cylinder at the MWL. (Note that allowing for forcing to be considered at *x(z,t)* via *u(x,z,t)* produces nonlinearities that normally have only a minor effect on the character of the response (Haritos, 1986)).

When equation (22) for *f(z,t)* is substituted into equation (23) above, the so-called "added mass" term is identified for the cylinder viz:

$$m' = \int_{-h}^{0} \frac{\pi}{4} \rho C_A D^2 \Psi^2(z)\, dz \qquad (24)$$

in which $C_A$ (= $C_M$ – 1) is the "added mass" coefficient.

This is an important result as it suggests that for all intensive purposes a body of fluid surrounding the cylinder appears to be "attached" to it in its inertial response, and hence the coining of the label "added mass" effect.

Equation (23) can be re-cast in the form

$$\ddot{x}_o + 2\omega_o \zeta_o \dot{x}_o + \omega_o^2 x_o = \frac{F_I(t) + F_D(t)}{m + m'} \qquad (25)$$

where

$$F_I(t) = \int_{-h}^{0} \alpha \dot{u}(z,t) \Psi(z)\, dz \qquad (26)$$

and

$$F_D(t) = \int_{-h}^{0} \beta.\big(u(z,t) - \dot{x}_o(t)\Psi(z)\big). \big|u(z,t) - \dot{x}_o(t)\Psi(z)\big|.\Psi(z).dz \qquad (27)$$

in which $\alpha = \frac{\pi}{4}\rho C_M D^2$ and $\beta = \frac{1}{2}\rho C_D D$, $\omega_o$ is the natural circular frequency of the first mode and $\zeta_o$ is the critical damping ratio of the structure in otherwise still water conditions.

In the case of $\Psi(z)\dot{x}_o(t)$ small compared to *u(z,t)* an approximation that can be made for this interactive term is of the form:

$$\big(u(z,t) - \dot{x}_o(t)\Psi(z)\big)\big|u(z,t) - \dot{x}_o(t)\Psi(z)\big| \approx u(z,t)\big|u(z,t)\big| - 2\big|u(z,t)\big|\dot{x}_o(t)\Psi(z) \qquad (28)$$

Under these circumstances, equation (25) can be further simplified to:

$$\ddot{x}_o + 2\omega_o\big(\zeta_o + \zeta_H\big)\dot{x}_o + \omega_o^2 x_o = \frac{F_I(t) + F'_D(t)}{m + m'} \qquad (29)$$

where

$$F'_D(t) = \int_{-h}^{0} \beta u(z,t)\big|u(z,t)\big|\Psi(z)\, dz \qquad (30)$$

which is interpreted as the level of equivalent drag force at the MWL in the case of rigid support conditions (negligible dynamic response).

The term $\zeta_H$ in equation (29) is the contribution to damping due to hydrodynamic drag interaction viz

$$\zeta_H \approx \frac{\int_{-h}^{0} \beta\big|\bar{u}(z,t)\big|\Psi^2(z)\, dz}{(m + m')\omega_o} \qquad (31)$$

(In the case of large diameter compliant cylinder in the diffraction forcing regime, analogous expressions can be derived for added mass effects and radiation damping due to structure-fluid interaction effects).

## 4 RESPONSE TO IRREGULAR SEA STATES

### 4.1 *Inertia Force*

Since the inertia force term $F_I(t)$ in equation (29) is linear it generally poses little difficulty in modelling under a variety of hydrodynamic conditions.

Consider an irregular sea state composed of a Fourier Series of Airy wavelets conforming to a P-M spectral description. Then $\dot{u}(z,t)$ can be obtained from the expression

$$\dot{u}(z,t) = \sum_{n=0}^{N/2} \left( \frac{-\omega_n^2 \cosh\big(\kappa_n(z+h)\big)}{\sinh(\kappa_n h)} \cdot \sqrt{\frac{2S_\eta(f)}{T}} \cos\left(\frac{2\pi n t}{T} - \phi_n\right) \right) \qquad (32)$$

in which $\kappa_n$ satisfies the dispersion relationship of equation (4).

In the case of $\Psi(z)$ being a power law profile, as in Figure 10, then

$$\Psi(z) = \left(1 + \frac{z}{h}\right)^N \qquad (33)$$

and $F_I(t)$ can be shown to be obtainable via the expression given by (Haritos, 1989),

$$F_I(t) = \frac{\pi}{4}\rho g C_M D^2 \sum_{n=0}^{N/2} \left( I_N(\kappa_n h). \sqrt{\frac{2.S_\eta(f)}{T}} \cos\left(\frac{2\pi n t}{T} - \phi_n\right)\right) \quad (34)$$

where:

$$I_N(\kappa_n h) = I_0(\kappa_n h) - \frac{N}{\kappa_n h}\left(1 - \frac{N-1}{\kappa_n h} I_{N-2}(\kappa_n h)\right), \; N \geq 2$$
$$I_0(\kappa_n h) = \tanh(\kappa_n h) \quad , N = 0 \quad (35)$$
$$I_1(\kappa_n h) = I_0(\kappa_n h) - \frac{1}{\kappa_n h}\left(1 - \frac{1}{\cosh(\kappa_n h)}\right) \quad , N = 1$$

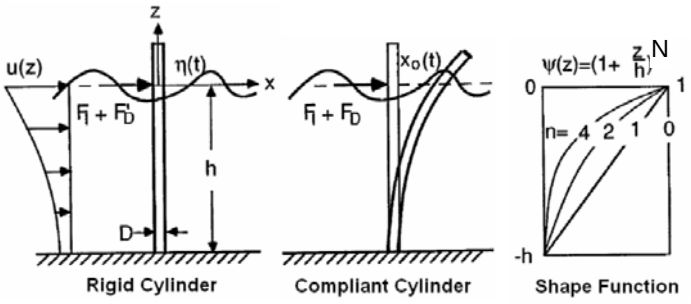


Figure 10: Compliant vertical surface-piercing cylinder

Figure 11 presents the variations in $I_N(\kappa_n h)$ for a range of power exponents N in mode shape Ψ(z). The result for N = 0 is consistent with the derivation for the inertia force component acting on a rigid cylinder due to an Airy wave made in Appendix I.

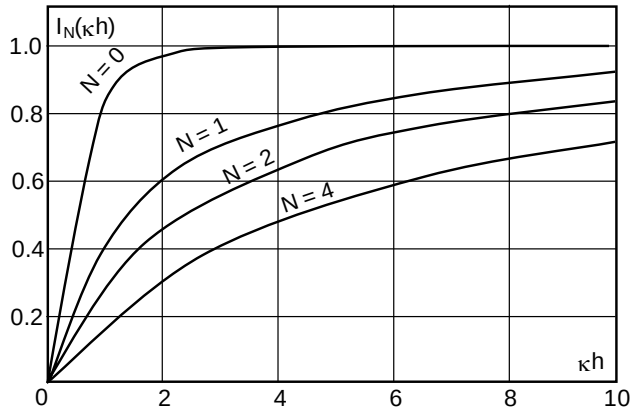


Figure 11: Variation of $I_N(\kappa h)$ for varying N

It is observed that all variations for $I_N(\kappa_n h)$ are asymptotic to 1 and that $I_0(\pi)$ is close to this value to the order of accuracy associated with the "deep water" limit of Airy waves (ie κh = π) but for N>0, $I_N(\kappa h) \approx 1$ for κh >> π. In general, the effect of higher order mode shapes (N > 0) is to reduce the level of inertia forcing of each Airy wavelet in an irregular sea state.

Figure 12 depicts the results obtained for the response of a vertical cylinder in deep water conditions ($I_N(\kappa h)$ = 1) for inertia only forcing in unidirectional P-M waves.

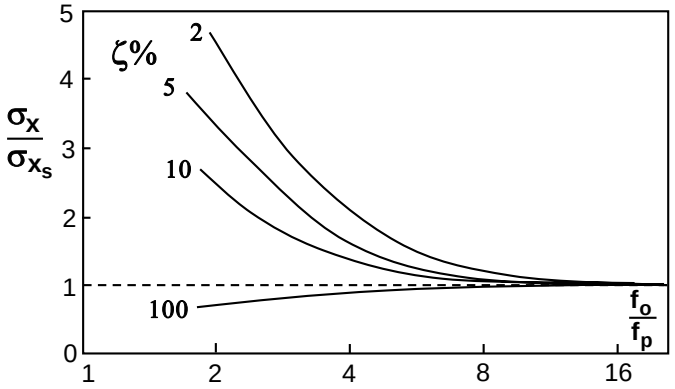


Figure 12: Influence of Dynamic Properties on Response (Inertia dominant forcing in deep water)

The levels are quoted as the ratio of the standard deviation in the response of a cylinder exhibiting a natural frequency of $f_o$ to that of a near weightless cylinder with the same stiffness for which $f_o$ approaches infinity. It is clear from direct observation of Figure 12, that response levels are controlled by both damping and the amount of relative energy available near 'resonance' for a dynamically responding cylinder in an irregular sea state.

## 4.2 *Drag force*

Whilst it is possible to deal with the $u|u|$ term for drag force numerically, the linearised approximation to $|\bar{u}(z,t)|$ attributed to Borgman (1967), can be used in the case *u(z,t)* Gaussian in a random sea state, so that

$$|\bar{u}(z,t)| \approx \sqrt{\frac{8}{\pi}}.\sigma_u(z) \quad (36)$$

where $\sigma_u(z)$ is the standard deviation in water particle velocity and where current is taken as zero-valued for all z.

This approximation can be used to simplify the expressions for both $\zeta_H$ in equation (31) and $F_D(t)$ in equation (30) and to thereby obtain closed-form solutions in the case of nominated $\Psi(z)$ variations.

This approximation would seem reasonable for determination of $\zeta_H$ for "stiff" structures, but in situations when the drag force $F_D(t)$ is considered dominant, this linearization can lead to significant errors in the modelling of both the non-linear drag force and the prediction of the resultant response, according to Lipsett (1985).

# 5 EXTREME VALUES

In the case of random vibrations associated with linear systems, use can be made of upcrossing theory

in combination with spectral modelling of the processes involved to develop a basis for prediction of peak response values, (Nigam & Narayanan, 1994).

A linear filter has the characteristics described by ($H_{y,\eta}(f)$, $\phi_{lag}(f)$) which apply to the Fourier components of a random time varying quantity (such as a waveheight trace, $\eta(t)$, conforming to say a P-M spectrum) at frequency $f$, to produce a modified resultant time varying quantity, $y(t)$, that is linearly related to $\eta(t)$, as follows

$$y(t) = \sum_{n=1}^{N/2} H_{y,\eta}(f_n). \left(a_n \cos\left(\frac{2\pi nt}{T} - \phi_{lag}(f_n)\right) + b_n \sin\left(\frac{2\pi nt}{T} - \phi_{lag}(f_n)\right)\right) \quad (37)$$

A 'zero-lag' filter would be one for which $\phi_{lag}(f_n) = 0$ for all frequencies $f_n$.

The spectrum for $y$, given by $S_y(f)$, can be obtained from the spectrum of waveheight, $S_\eta(f)$, via

$$S_y(f) = H^2_{y,\eta}(f).S_\eta(f) \quad (38)$$

## 5.1 *Extreme Wave Forces*

Use can be made of the dispersion relationship of equation (4) in conjunction with the separate descriptions above for Inertia and Drag force, to obtain the associated relationships for $H_{F_I,\eta}(f)$ and $H_{F_D,\eta}(f)$ respectively, and hence the total force spectrum for the surface-piercing cylinder of Figure 6. A diagrammatic illustration of the concept is provided in Figure 13.

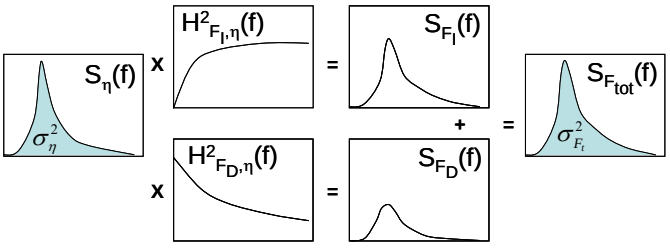


Figure 13: Diagrammatic description of spectral modelling of Morison wave loading

The area under the total force spectrum equals the variance, $\sigma^2_{F_T}$, knowledge of which may be used to estimate peak Morison loading of the vertical surface-piercing cylinder, under consideration. This peak load value may reasonably be expected to be of the order $3\sigma_{F_T}$, but a more precise estimation is offered through the use of upcrossing theory.

For a Normally distributed trace $y(t)$ with zero mean and variance $\sigma^2_y$, the rate of upcrossings at level $y$, $\nu_y$, equates to the count of upcrossings at level $y$, $N_y$, divided by the time length of trace, T (ie $\nu_y = N_y/T$). $\nu_o$ would correspond to the rate of upcrossings of the zero mean.

It can be shown (Newland, 1975) that upcrossings for such a trace would satisfy

$$\frac{\nu_y}{\nu_o} = \frac{N_y}{N_o} = e^{-\frac{1}{2}\left(\frac{y}{\sigma_y}\right)^2} \quad (39)$$

The concept of a "peak value" in a time period of T would correspond to a $y$ value with an upcrossing count of 1 so that $y_{max}$ can be estimated from

$$\frac{1}{\nu_o T} = e^{-\frac{1}{2}\left(\frac{y_{\max}}{\sigma_y}\right)^2} \quad (40)$$

so that

$$y_{\max} = \sqrt{2\ln(\nu_o T)}.\sigma_y \quad (41)$$

Because the value of $y_{max}$ itself shows a statistical variation, Davenport (1964) has suggested a small correction to equation (41) for the value of $E(y_{max})$ so that

$$y_{\max} = \left(\sqrt{2\ln(\nu_o T)} + \frac{0.577}{\sqrt{2\ln(\nu_o T)}}\right).\sigma_y \quad (42)$$

Now the rate of "zero" upcrossings is given by:

$$\nu_o = \frac{\left(\frac{\sigma(\dot{y})}{\sigma(y)}\right)}{2\pi} = \sqrt{\frac{\int_0^\infty f^2 S_y(f)\,df}{\int_0^\infty S_y(f)\,df}} \quad (43)$$

which can be determined from the spectral description. If $y(t)$ is a narrow-banded process (ie energy is concentrated at a peak frequency, $f_p$), then $\nu_o \approx f_p$.

## 5.2 *Extreme Response Values*

The concepts above can be applied to the dynamically responding surface-piercing cylinder to estimate the peak response at MWL, $(x_o)_{max}$.

An additional stage is required for this purpose, namely the linear transformation from Morison forcing to dynamic excitation via the description of equation (29), which in terms of a spectral modelling approach, is diagrammatically depicted in Figure14.

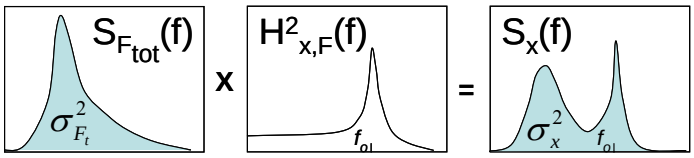


Figure 14: Diagrammatic description of spectral modelling of dynamic response

The Transfer Function for response from Morison loading in irregular sea states for the dynamically responding surface-piercing cylinder of Figure 10 is given by $H_{x,F}(f)$, via

$$H^2_{x,F}(f) = \frac{\chi^2_m(f)}{(m+m')^2} \tag{44}$$

where

$$\chi^2_m(f) = \frac{1}{\left(\left(1-\left(\frac{f}{f_o}\right)^2\right)^2 + \left(2\zeta_{tot}\left(\frac{f}{f_o}\right)\right)^2\right)} \tag{45}$$

in which $f_o$ is the natural frequency of the cylinder and $\zeta_{tot}$ is the total critical damping ratio ($\zeta_{tot} = \zeta_o + \zeta_H$).

The area under the response spectrum yields $\sigma_x^2$ and after application of equation (43) to obtain $\nu_o$, extreme value $(x_o)_{max}$ can be obtained from equation (42), for the nominated duration of the irregular sea state under consideration, (eg T = 3600 secs for a 1-hour storm).

## 6 CONCLUDING REMARKS

This paper has provided an overview of some of the key factors that need be considered in the analysis and design of offshore structures. Emphasis has been placed on modelling of the hydrodynamic response of a compliant vertical surface-piercing cylinder in the Morison loading regime under uni-directional waves. Reference has also been made to a number of publications in which further detail and extension of treatment can be explored by the interested reader.

## REFERENCES

API, 1984. *Recommended Practice for Planning, Designing and Constructing Fixed Offshore Platforms*, American Petroleum Institute, API RP2A, 15th Edition.

Borgman, L.E. 1967. Spectral Analysis of Ocean Wave Forces on Piling, *Jl WW& Harbors*, Vol. 93, No. WW2, pp 129-156.

Davenport, A.G. 1964. Note on the Distribution of the Largest Value of a Random Function with Application to Gust Loading, *Proc. ICE*, Vol. 28, No. 187.

DNV-OS-C101, 2004. *Design of Offshore Steel Structures, General (LFRD Method).* Det Norske Veritas, Norway.

DNV-OS-C105, 2005. *Structural Design of TLPS, (LFRD Method)*. Det Norske Veritas, Norway.

DNV-OS-C106, 2001. *Structural Design of Offshore Deep Draught Floating Units, (LFRD Method)*. Det Norske Veritas, Norway.

Chakrabarti, S. K. (ed) 2005. *Handbook of Offshore Engineering*, San Francisco: Elsevier.

Chakrabarti, S. K. 2002. *The Theory and Practice of Hydrodynamics and Vibration*, New Jersey: World Scientific.

Chakrabarti, S. K. (ed) 1987. *Fluid Structure Interaction in Offshore Engineering*, Southampton: Computational Mechanics Publications.

Chakrabarti, S. K. 1994. *Hydrodynamics of Offshore Structures*, Southampton: Computational Mechanics Publications.

Dean R. G. & Dalrymple, R. A. 1991. *Water Wave Mechanics for Engineers and Scientists*, New Jersey: World Scientific.

Rienecker, M.M. & Fenton, J.D. 1981. A Fourier approximation method for steady water waves, *J. Fluid Mechs*, Vol 104, pp 119-137.

Graff, W. J. 1981. *Introduction to Offshore Structures – Design, Fabrication, Installation*, Houston: Gulf Publishing Company.

Haritos, N. 1986. Nonlinear Hydrodynamic Forcing of Buoys in Ocean Waves, *Proc. 10th Aust. Conf. on Mechs. of Structs. & Materials*, Adelaide, pp 253-258.

Haritos, N. 1989. The Influence of Modal Characteristics on the Dynamic Response of Compliant Cylinders in Waves, *Computational Techniques & Applications: CTAC-89*, edit W.L. Hogarth & B.J. Noye, pp 683-690, (Hemisphere).

Holand, I., Gudmestad, O. T. & Jersin, E. (eds). 2000. *Design of Offshore Concrete Structures*, London: Spon Press.

ICE, 1983, Design in Offshore Structures, ICE, London: Thomas Telford Ltd.

Le Mehaute, B. 1969. An introduction to hydrodynamics and water waves, *Water Wave Theories*, Vol. II, TR ERL 118-POL-3-2, U.S. Department of Commerce, ESSA, Washington, DC.

Lipsett, A.W. 1985. Nonlinear Response of Structures in Regular and Random Waves, *Ph.D. Thesis, Univ. of British Columbia*, Canada.

MacCamy, R. C. & Fuchs, R.A.1954. Wave Forces on Piles: a Diffraction Theory, *U.S. Army Coastal Engineering Centre*, Tech Memo No. 69.

Newland, D.E. 1975. *An Introduction to Random Vibrations and Spectral Analysis*. Longman.

Nigam, N. C. & Narayanan, S. 1994. *Applications of Random Vibrations*, New York: Springer-Verlag.

Sarpkaya, T. 1976, In-line and transverse forces on cylinders in oscillating flow at high Reynold's number, *Proc. 8th Offshore Technology Conference*, Houston, Texas, OTC 2533, pp 95-108.

Sarpkaya, T. & Isaacson, M. 1981. *Mechanics of Wave Forces on Offshore Structures*, New York: Van Nostrand

SESAM, **http://www.dnv.com/software/systems/sesam/programModules.asp**

Stewart, R. H. 2006. Introduction to Physical Oceanography, http://oceanworld.tamu.edu/resources/ocng_textbook/PDF_files/book.pdf.

WAMIT, **http://www.wamit.com/**

Wheeler, J.D. 1970. Method for calculating forces produced by irregular waves, *Journal of Petroleum Technology*, March, pp 359-367.

## Appendix I. – Base shear on a surface-piercing cylinder from Morison loading

$$f(z,t) = f_I(z,t) + f_D(z,t)$$

$$f_I(z,t) = \alpha\, \dot{u} \quad ; \quad (\alpha = \frac{\pi}{4}\, \rho\, C_M\, D^2)$$

$$f_D(z,t) = \beta\, u|u| \quad ; \quad (\beta = \frac{1}{2}\, \rho\, C_D\, D)$$

**Inertia:**

$$F_I(t) = \int_{-h}^{o} \alpha\, \dot{u}\, dz \quad \left( = \int_{-h}^{o} f_I(z,t)\, dz \right)$$

$$= \alpha\, \frac{\omega^2}{\sinh(\kappa h)}\, a.\sin(\kappa x - \omega t) \left| \frac{\sinh(\kappa(z+h))}{\kappa} \right|_{-h}^{o}$$

$$= \alpha\, \frac{\omega^2}{\kappa}\, a\, .\, \sin(\kappa x - \omega t) \left| \frac{\sinh(\kappa h)}{\sinh(\kappa h)} - 0 \right|$$

$$= \alpha\, g \tanh(\kappa h)\, .\, a\, .\, \sin(\kappa x - \omega t)$$

$$= \alpha\, g\, a \sin(\kappa x - \omega t) \qquad \textit{(Deep Water)}$$

**Drag:**

$$F_D(t) = \int_{-h}^{o} \beta\, u|u| dz \quad \left( = \int_{-h}^{o} f_D(z,t)\, dz \right)$$

$$= \beta\, \frac{a^2\, \omega^2}{\sinh^2 \kappa h} \cos(\kappa x - \omega t)\, |\cos(\kappa x - \omega t)| \; . \int_{-h}^{o} \cosh^2(\kappa(z+h))\, dz$$

$$F_D(t) = \beta\, \frac{a^2\, \omega^2}{\sinh^2(\kappa h)} \cos(\kappa x - \omega t)\, |\cos(\kappa x - \omega t)| \; . \int_{-h}^{o} \frac{1}{2}(1 + \cosh 2(\kappa(z+h)))\, dz$$

$$F_D(t) = \beta\, \frac{a^2\, \omega^2}{\sinh^2(\kappa h)} \cos(\kappa x - \omega t)\, |\cos(\kappa x - \omega t)| \; . \; \frac{1}{2}\left(h + \frac{\sinh(2\kappa h)}{2\kappa}\right)$$

$$F_D(t) = \left[ \beta\, \frac{a^2\, \omega^2\, h}{2 \sinh^2(\kappa h)} + \beta\, \frac{a^2\, g \tanh(\kappa h)}{4} \left( \frac{\sinh(2\kappa h)}{\sinh^2(\kappa h)} \right) \right] . \cos(\kappa x - \omega t)|\cos(\kappa x - \omega t)|$$

$$= \left[ \beta\, \frac{a^2 g\, \kappa h}{\sinh 2\kappa h} + \beta\, \frac{a^2 g}{2} \right] \cos(\kappa x - \omega t)|\cos(\kappa x - \omega t)|$$

$$= \frac{\beta\, a^2 g}{2} \left[ \frac{2\, \kappa\, h}{\sinh 2\kappa h} + 1 \right] \cos(\kappa x - \omega t)|\cos(\kappa x - \omega t)|$$

Hence, as an alternative approximation

$$F_D(t) \approx \frac{\beta\, a^2 g}{2} \cos(\kappa x - \omega t)$$

**Inertia:**

$$\alpha\; a\, g \tanh(\kappa h) \sin(\kappa x - \omega t) \rightarrow F_I \sin(\kappa x - \omega t)$$

**Drag:**

$$\frac{\beta\, a^2 g}{2} \left[ \frac{2\, \kappa\, h}{\sinh 2\kappa h} + 1 \right] \cos(\kappa x - \omega t)\, .\, |\cos(\kappa x - \omega t)|$$

$$\rightarrow F_D \cos(\kappa x - \omega t)\, |\cos(\kappa x - \omega t)|$$

Figures I.a and I.b depict representative variations over one cycle of Airy wave of the Base Shear force acting on a cylinder normalised with respect to $F_D/F_I = 2$, respectively, by way of illustration.

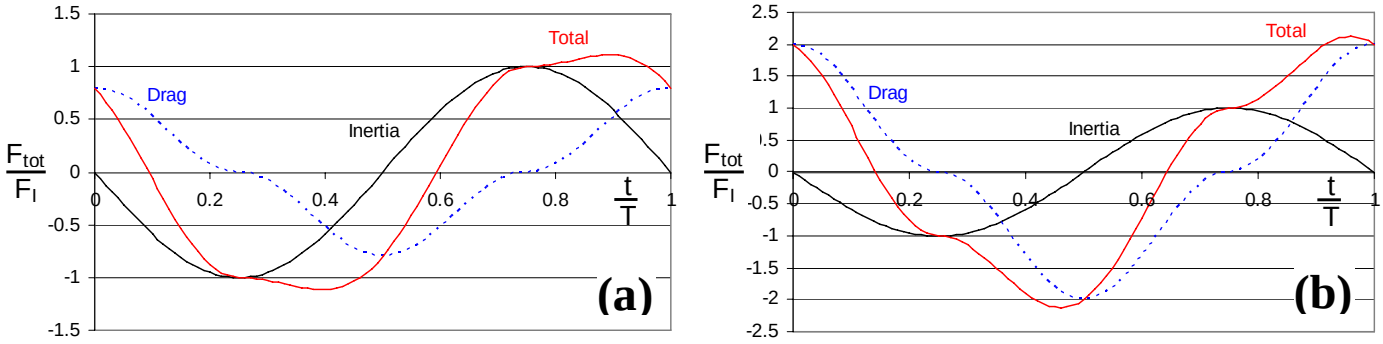


Figure I: Morison Base Shear Force components for (a): $F_D/F_I = 0.8$ and (b): $F_D/F_I = 2$